3D SIMULATION OF HIGH-VELOCITY IMPACT DAMAGE PROGRESS IN THE CFRP LAMINATES

A. Yoshimura[1*], K. Nagakura[2], T. Okabe[3], H. Kusano[4], M. Yamada[5], Y. Tanabe[5], T. Ogasawara[1], H. Nakatani[2], S. Ogihara[2]

[1] *Advanced Composite Research Center, Japan Aerospace Exploration Agency, 6-13-1 Osawa, Mitaka, Tokyo 181-0015, JAPAN*
[2] *Faculty of Science and Technology, Tokyo University of Science, 2641 Yamazaki, Noda, Chiba 278-8510, JAPAN*
[3] *School of Engineering, Tohoku University, 6-6 Aoba, Aramaki, Aoba-ku, Sendai, Miyagi 980-8579, JAPAN*
[4] *Shimadzu Corporation, 1 Nishinokyo-Kuwabata-cho, Nakagyo-ku, Kyoto 604-8511, JAPAN*
[5] *Graduate School of Engineering, Nagoya University, Furo-cho, Chikusa-ku, Nagoya, Aichi 464-8601, JAPAN*
**Corresponding Author (yoshimura.akinori@jaxa.jp)*

Keywords: CFRP, High velocity impact, Finite element analysis, Damage simulation

t

Abstract

In the present paper, an analytical model which simulates the damage process of carbon fiber reinforced plastics (CFRP) under high velocity impact is proposed. The simulation model is based on the finite element method, in which the damage is considered by using stress criterion, continuum damage mechanics (CDM), and cohesive zone model (CZM). The parameters of the stress criterion, CDM and CZM, such as tensile strength and interlaminar toughness, are determined by the experimental results of the static tests, and there is no fitting parameter. The simulated damage agrees very well with the experimental damage observation.

1 Introduction

Structural weight reductions of civil aircraft engines are demanded in order to reduce the emission of CO_2. Applications of carbon fiber reinforced plastics (CFRP) to structures of turbofan engines can significantly reduce their weight. CFRPs are potentially applicable to the fan system which includes fan blades and fan cases, because the environmental temperature of the fan system is relatively low. In some engines, CFRPs have already been used [1].

For fan systems of aircraft engines, one of the most serious technical problems is foreign object damage (FOD), which means the damage caused by the foreign objects which are ingested into engines. Because fan systems are located at front of the engines, foreign objects, such as birds, directly collide against the fan blades. And the broken fan blades collide against the fan case. The impact velocities of these events are about 100-500 m/s. Therefore, for the design of the CFRP fan system, investigations of high velocity impact properties of CFRP laminates are essential.

Results of high velocity impact tests were already published by several researchers [2-5]. Tanabe et al. [5] conducted high velocity impact tests for CFRPs which consist of various carbon fibers and matrices, moreover, properties of fiber/marix interfaces were also varied.

They revealed that these properties significantly affected ballistic limits of the CFRP laminates. Therefore, we believe that the analytical model which can predict high velocity impact behaviors of CFRP laminates based on the properties of fibers, matrices and interfaces is necessary for deeper understanding of the ballistic limits. However, to author's knowledge, there are not such analytical models.

In the present study, we propose a numerical analytical model which simulates the damage process of CFRP under high velocity impact. The model is based on three dimensional explicit finite element method, in which damages are introduced. Criteria of the damages are decided using static tests results because they are affected by the properties of the fibers, matrices and interfaces, and because they can easily be measured. This paper is organized as follows. In Section 2, the experimental results of the high velocity impact tests are briefly reported. In Section 3, the formulation of the simulation model is described. In Section 4, we show the simulation results and compare them with experimental results. Conclusions from the present study are drawn in the last section.

2 High Velocity Impact Tests

Prior to the simulation, high velocity impact tests were performed. For the specimens, IMS60/#133 prepreg (Toho Tenax Co., Ltd) was employed. IMS60 is a middle-modulus and high-strength carbon fiber. #133 is a toughened epoxy resin system. Cross-ply $[0/90]_{4s}$ and quasi-istotropic $[45/0/-45/90]_{2s}$ specimens were tested. Figure 1 shows the dimensions of the specimen. The specimens were cut into 70 mm × 70 mm squares using a diamond-wheel cutter. Nominal thicknesses of both types of specimens were 2.2 mm. The specimens were gently clamped by the base plate and the holder plate so as not to fall down. These plates had 60 mm × 60 mm square windows (see Fig. 1).

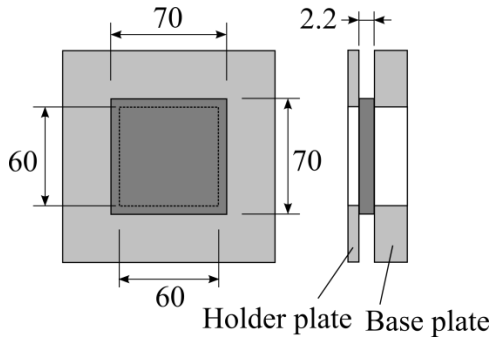

Figure 1. Dimensions of the specimen and fixtures.

The projectile used was a bearing-steel sphere of diameter was 6.0 mm (mass=0.9 g). The projectile was supported by the sabot, and was accelerated by a single-stage gas-gun. The projectile perpendicularly collided at the center of the specimen. The impact velocity was controlled by changing the gas pressure. The impact velocity was measured using images of a high-speed camera.

The bottom surface of the specimen was photographed by two high-speed cameras every 4μs during the impact (see Fig. 2). Using the digital image correlation (DIC) method, distributions of three-dimensional displacement were calculated. The detailed measurement method is found in the published paper [6]. The results of DIC will be described in Section 4.

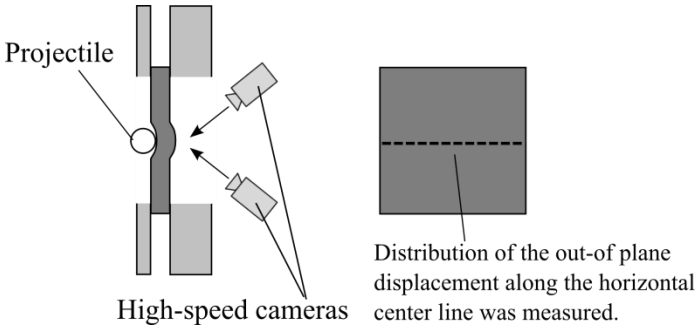

Figure 2. Schematic showing digital image correlation (DIC) method.

After the impact tests, two kinds of X-ray non-destructive inspections (NDI) were conducted. We took soft X-ray radiographs using general-purpose X-ray film device (SV-100AW, SOFTEX, Inc.) in order to observe the in-plane distributions of the damages. In addition, we took section images by soft X-ray micro-focus computed tomography (CT) system (TOSCANER-30000μhd, TOSHIBA IT & Control Systems Corp.) in order to observe through- the-thickness damage distributions. Figures 3 and 4 show the X-ray radiographs and X-ray CT images. We can clearly see the ply cracks (transverse and shear cracks), and delaminations in Fig. 3, and also see the fiber failures in Fig. 4.

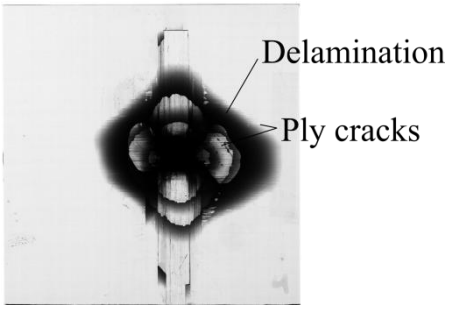

Figure 3. Soft X-ray radiograph of the cross-ply specimen (impact velocity=186 m/s)

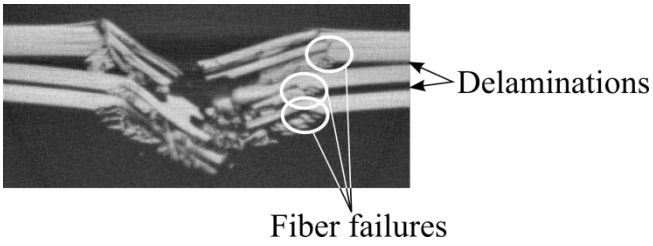

Figure 4. X-ray computed tomography of the cross-ply specimen (impact velocity=186 m/s)

3 Simulation Model

Experimental observations revealed that the high velocity impact caused three types of damages in the CFRP laminates: fiber failures, transverse cracks and delaminations. In this section we propose a numerical simulation model. The model is based on the explicit finite element analysis. The CFRP laminate was divided into laminae, and the lamina was divided by 8-node brick elements. Fig. 5 shows the coordinate system of single element.

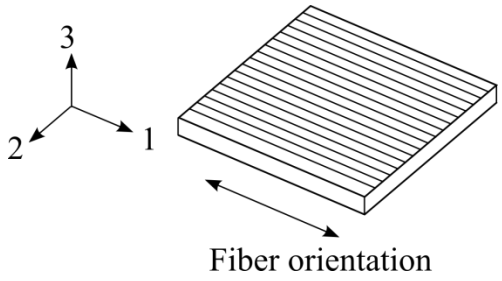

Figure 5. Coordinate system of the single element

Each type of damage was introduced in each manner. Fiber failures were judged by simple stress criteria in each element. In order to model the tensile failure, when the fiber direction tensile stress σ_1 and the out-of-plane shear stress τ_{13} satisfy

$$\left(\frac{\langle\sigma_1\rangle}{S_L{}^T}\right)^2+\left(\frac{\tau_{13}}{S_{LT}}\right)^2=1, \tag{1}$$

the element was vanished from the analysis. $S_L{}^T$ and $S_L{}^T$ denote the fiber-direction tensile strength and out-of-plane shear strength of the CFRP laminate.

Angle bracket means $\langle x\rangle=0$ when $x<0$, and $\langle x\rangle=x$ when $x\geq 0$. On the other hand, fiber compressive failure was determined by

$$\left(\frac{\langle-\sigma_1\rangle}{S_L{}^C}\right)=1 \tag{2}$$

where $S_L{}^C$ denotes the compressive strength of the CFRP in fiber direction. Once the element satisfied the condition, the stiffness of the element in fiber direction was decreased to zero. The tensile and compressive strengths were determined using the results of fiber-direction tensile and compressive tests.

Transverse cracks are modeled using continuum damage mechanics (CDM) [7,8]. The conventional formulation of CDM usually uses effective stress, which means the stress enlarged by distributed damages. However, in this study, we used effective strain tensor $\tilde{\boldsymbol{\varepsilon}}$ instead of the effective stress. The effective strain tensor $\tilde{\boldsymbol{\varepsilon}}$ is calculated from the strain tensor $\boldsymbol{\varepsilon}$ as,

$$\tilde{\boldsymbol{\varepsilon}}=\frac{1}{2}\left\{(\boldsymbol{I}-\boldsymbol{D})\boldsymbol{\varepsilon}+\boldsymbol{\varepsilon}(\boldsymbol{I}-\boldsymbol{D})\right\} \tag{3}$$

where $\boldsymbol{I}$ and $\boldsymbol{D}$ denote the second-order unit tensor and the damage tensor, respectively. In this study, the damage tensor $\boldsymbol{D}$ is defined by

$$\boldsymbol{D}=d_2\,\boldsymbol{n}_2\otimes\boldsymbol{n}_2 \tag{4}$$

where $\boldsymbol{n}_2$ denotes the unit vector (see Fig. 5), and d_2 is a damage parameter. d_2 is initially equal to 0 (intact), and it gradually increases according to the damage evolution. Finally it becomes equal to 1 when complete failure occurs. Using the effective strain, the stress tensor $\boldsymbol{\sigma}$ is then calculated as,

$$\boldsymbol{\sigma}=\boldsymbol{C}\tilde{\boldsymbol{\varepsilon}}=\frac{1}{2}\boldsymbol{C}\left[(\boldsymbol{I}-\boldsymbol{D})\boldsymbol{\varepsilon}+\boldsymbol{\varepsilon}(\boldsymbol{I}-\boldsymbol{D})\right] \tag{5}$$

where $\boldsymbol{C}$ denotes elastic stiffness tensor. Using Eqs. (4) and (5), strain energy per unit volume e is calculated as,

$$e=\frac{1}{2}\Big[C_{11}{\varepsilon_{11}}^2+(2-d_2)C_{12}\varepsilon_{11}\langle\varepsilon_{22}\rangle+2C_{12}\varepsilon_{11}\langle-\varepsilon_{22}\rangle+2C_{13}\varepsilon_{11}\varepsilon_{33}+(1-d_2)C_{22}\langle\varepsilon_{22}\rangle^2+C_{22}\langle-\varepsilon_{22}\rangle^2+$$
$$(2-d_2)C_{23}\langle\varepsilon_{22}\rangle\varepsilon_{33}+2C_{23}\langle-\varepsilon_{22}\rangle\varepsilon_{33}+C_{33}{\varepsilon_{33}}^2+(1-d_2/2)C_{44}{\gamma_{12}}^2+C_{55}{\gamma_{13}}^2+(1-d_2/2)C_{66}{\gamma_{23}}^2\Big] \quad (6)$$

where C_{xy} denotes xy components of stiffness tensor. Let Y_2 be the thermodynamic conjugate parameter of d_2. Y_2 can be calculated by partially differentiating the specific elastic energy e by d_2,

$$Y_2=-\frac{\partial e}{\partial d_2}=\frac{1}{2}\Big[C_{12}\varepsilon_{11}\langle\varepsilon_{22}\rangle+C_{22}\langle\varepsilon_{22}\rangle^2+C_{23}\langle\varepsilon_{23}\rangle\varepsilon_{33}+\frac{1}{2}C_{12}{\gamma_{12}}^2+\frac{1}{2}C_{23}{\gamma_{23}}^2\Big] \quad (7)$$

In this study, the damage evolution law $d_2=f(Y_2)$ was determined by using static tensile test results of $[0/90_3]_s$ specimens [9] (see Fig. 6). Figure 7 shows the flow chart of the CDM model in the explicit finite element analysis.

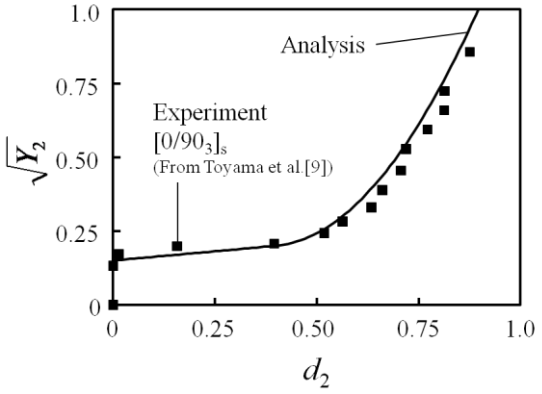

Figure 6. Damage evolution law ($d2$-$Y2$ relationship)

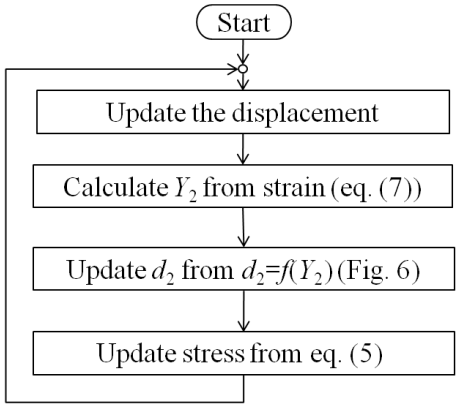

Figure 7. Flowchart of the CDM analysis

Delaminations were modeled by introducing cohesive elements into each ply interface. Maximum tractions of cohesive elements were determined by using 90° tensile and short beam shear tests results. The absorbed energies by cohesive elements were determined by DCB and ENF tests.

Figure 8 shows an overview of the simulation model. Jig and projectile were modeled by rigid surface. The diameter of the projectile was 6.0 mm, the mass was 0.9 g. The stacking sequences analyzed were cross-ply $[0/90]_{4s}$ and quasi-isotropic $[45/0/-45/90]_{2s}$. It should be noted that only a quarter of the model was analyzed in the case of the cross-ply model, because of the laminate's symmetry. General-purpose finite element code ABAQUS Explicit 6.8-3 was employed for analysis. Fiber failures and ply cracks were introduced using user

subroutine VUMAT. Delaminations were modeled using ABAQUS's built-in cohesive elements.

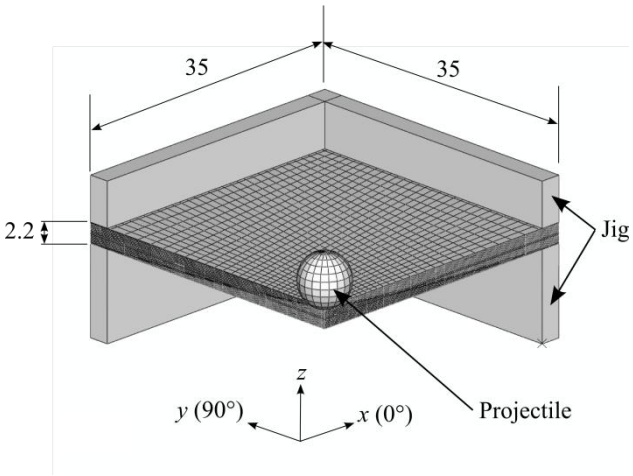

Figure 8. An overview of the simulation model for cross-ply laminates. For quasi-isotropic laminates, the whole laminates were analyzed, the mesh divisions of both models were the same.

4 Simulation Results

The material properties used in the simulation are shown in Table 1. The comparison of damage areas between experimental and simulation results of the cross-ply laminate is shown in Fig. 9. In the experiment, circular delamination occurred at the center of the specimen. In addition, long ply crack occurred along 0° direction at the bottom of the specimen, and the delamination extended along the crack at the bottom of the specimen because of the stress concentration around the crack tip. The simulation well predicted the circular delamination at the center of the laminate. Because the stress concentration did not appear in the continuum damage mechanics, the long delamination at the bottom of the laminate did not occurr in the simulation. Figure 10 shows the comparison of damage areas of the quasi-isotropic laminates. The simulation well predicted the damage area.

Longitudinal Young's modulus E_1 (GPa)	165.0
Transeverse Young's modulus E_2 (GPa)	7.73
Out-of-plane Young's modulus E_3 (GPa)	7.73
In-plane shear modulus G_{12} (GPa)	3.83
Out-of-plane shear modulus G_{23} (GPa)	3.40
Out-of-plane shear modulus G_{31} (GPa)	3.83
In-plane Poisson's ratio v_{12}	0.326
Out-of-plane Poisson's ratio v_{23}	0.450
Out-of-plane Poisson's ratio v_{13}	0.326
Fiber direction tensile strength $S_L{}^T$ (MPa)	2732
Fiber direction compressive strength $S_L{}^C$ (MPa)	1037
Mode I interlaminar maximum traction σ_{max} (MPa)	65.0
Mode II interlaminar maximum traction τ_{max} (MPa)	100.0
Mode I interlaminar fracture toughness G_{Ic} (J/m^2)	435
Mode II interlaminar fracture toughness G_{IIc} (J/m^2)	1855

Table 1. Material properties used in the simulation

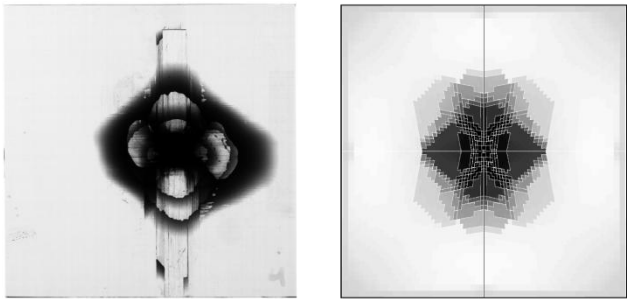

(a) Experiment (b) Simulation

Figure 9. Simulated and experimentally obtained delamination of the cross-ply laminates. Imapact velocity = 189 m/s.

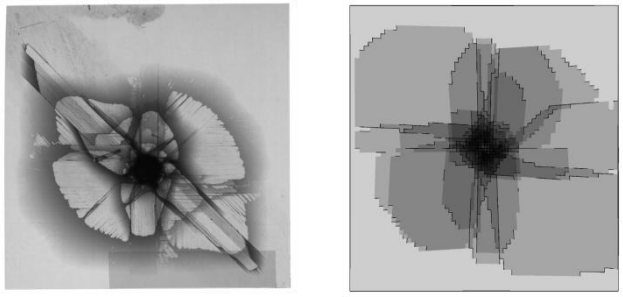

(a) Experiment (b) Simulation

Figure 10. Simulated and experimentally obtained delamination of the quasi-isotropic laminates. Impact velocity = 192 m/s (Experiment), 188 m/s (Simulatuion).

Figures 11 and 12 compare out-of-plane displace-ment distributions of the bottom surfaces of the impacted laminates. Horizontal axis corresponds to distance from the central point on the central line (see Fig. 2). Vertical axis shows out-of-plane displacements of the bottom surface. Points denote experimental results, which were obtained by DIC method. Simulation and experimental results agreed very well.

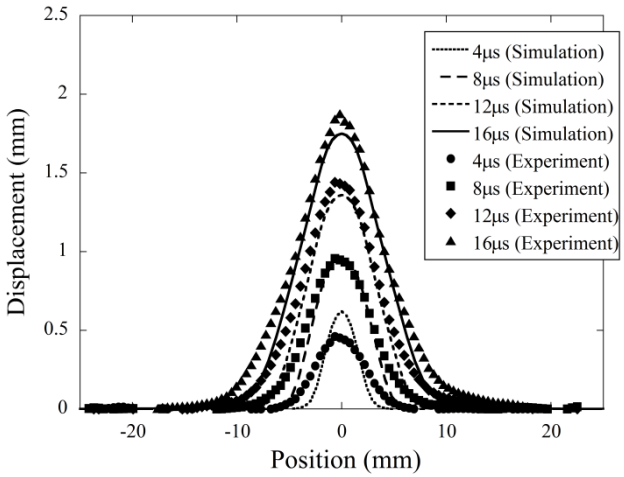

Figure 11. Comparison of the simulated and experimentally obtained out-of-plane displacement of the cross-ply laminate. Impact velocity=189 m/s

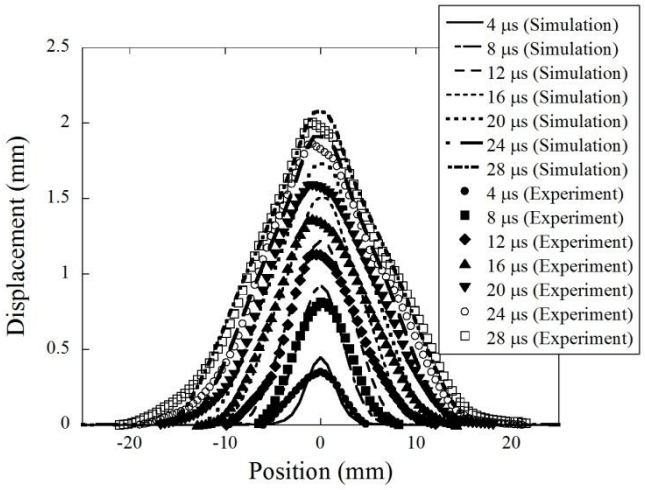

Figure 12. Comparison of the simulated and experimentally obtained out-of-plane displacement of the quasi-isotropic laminate. Impact velocity=149 m/s

The comparison between simulation and experimental results described above revealed that the simulation model which was proposed in this paper can well predict the high-velocity impact damage processes of the CFRP laminates.

5 Conclusion

In the present study, we proposed a new simulation model which simulates the damage process of CFRP under high velocity impact. It is based on the three-dimensional explicit finite element model. Three types of the damages: fiber failures, ply cracks and delaminations were introduced in the model. The model was verified by comparing the simulation results with test results. The results revealed that the model can well predict the high-velocity impact damage process of the CFRP laminates.

References

[1] Mecham, M., Composite power, *Aviation week and space technology*, pp.48-52, Apr. 17 (2006).

[2] Lopez-Puente, J., Zaera, R. and Navarro, C. An analytical model for high velocity impacts on thin CFRPs woven laminated plates. *Int. J. Solid. Struct.*, Vol. 44, pp. 2837-2851 (2007).

[3] Lopez-Puente, J., Zaera, R. and Navarro, C., Experimental and numerical analysis of normal and oblique ballistic impacts on thin carbon/epoxy woven laminates. *Composites Part A*, Vol. 39A, pp. 374-387 (2008).

[4] Caprino, G., Lopresto, V. and Santoro, D., Ballistic impact behavior of stitched graphite/epoxy laminates. *Compos. Sci. Technol.*, Vol. 67, pp. 325-335 (2007).

[5] Tanabe, Y., Aoki, M., Fujii, K., Kasano, H. and Yasuda, E., Fracture behavior of CFRPs impacted by relatively high-velocity steel sphere. *Int. J. Impact Eng.*, Vol. 28, pp. 627-642 (2003).

[6] Yamada, M., Tanabe, Y., Yoshimura, A. and Ogasawara, T., Three-dimensional measurement of CFRP deformation during high-speed impact loading. *Nucl. Instrum. Methods Phys. Res. A*, Vol. 646, pp.219-226 (2011).

[7] Skrzypek, J. and Ganczarski, A., *Modeling of Material Damage and Failure of Structures.* Springer, Berlin, (1999).

[8] Lubineau, G. and Ladevèze, P., Construction of a micromechanics-based intralaminar meso-model, and illustrations in ABAQUS/Standard. *Comput. Mater. Sci.*, Vol. 43, pp. 137-145 (2008).

[9] Toyama, N., Noda, J. and Okabe T., Quantitative damage detection in cross-ply laminates using Lamb wave method. *Compos. Sci. Technol.*, Vol. 63, pp. 1473-1479 (2003).